JOINT EUROPEAN TORUS JET

JET–P(93)01

L-G. Eriksson, T. Hellsten, U. Willen

A Comparison of Time Dependent Simulations with Experiments in Ion Cyclotron Heated Plasmas

A Comparison of Time Dependent Simulations with Experiments in Ion Cyclotron Heated Plasmas

L-G. Eriksson, T. Hellsten[1], U. Willen[2]

JET-Joint Undertaking, Culham Science Centre, OX14 3DB, Abingdon, UK

[1]Royal Institute of Technology, Stockholm, Sweden.
[2]Chalmers University of Technology, Gothenburg, Sweden.

Preprint of a Paper to be submitted for publication in Fusion Engineering and Design March 1999

A Comparison of Time Dependent Simulations with Experiments in Ion Cyclotron Heated Plasmas.

L.-G. Eriksson, T. Hellsten[+] and U. Willén[*].

JET-Joint Undertaking, Abingdon, Oxon, OX14 3EA, U.K..
[+]Royal Institute of Technology, S-100 44 Stockholm, Sweden.
[*]Chalmers University of Technology, S-412 96 Gothenburg, Sweden.

ABSTRACT

Comparisons between time dependent simulations and experiments in ion cyclotron heated plasmas in the JET tokamak have been done. The heating is simulated with a time dependent code, PION-T. The scenario which has been analyzed is minority heating of hydrogen at the fundamental cyclotron resonance in a deuterium majority plasma. For the analyzed scenario both second harmonic deuterium heating and fundamental hydrogen cyclotron heating take place. For large power, anisotropic high energy tails will be formed on the velocity distribution of the resonating ion species. The formation of such a tail on the deuterium is assessed by monitoring the 2.4 MeV neutron flux from (D,D) reactions. By taking the difference between two different plasma energy measurements, which put different weights on the parallel and perpendicular energy, the anisotropic energy content can be measured. This is compared with that calculated for hydrogen and deuterium. For low power levels or at the beginning of the heating pulse good agreement between calculations and measurements is found supporting that the power deposition is correctly described and that the fast ions, responsible for the anisotropic energy, slow down by classical collisions. For large amount of coupled power or later in the heating phase a clear difference between calculations and measurements is found. This discrepancy is identified, in the analyzed discharges, to be caused by finite orbit effects. By including the width of the drift orbits, good agreement between simulations and experiments is obtained also for the high power cases. Fast ions

have earlier been seen to be expelled from the centre of the plasma in connection with sawtooth crashes. By studying the rapid changes in fast energy content in connection with sawtooth instabilities we find the reduction to be consistent with that about 40% of the fast ions are expelled from the central region to the outside of the q=1 surface and that prompt losses are negligible.

1. INTRODUCTION

During recent years, ion cyclotron resonance heating (ICRH) has developed into a reliable heating method for large tokamak plasmas. Modelling of ICRH has also developed to include time depended calculations [1] and effects of real drift orbits [2] i.e. effects caused by that a drift orbit does not coincide with a single flux surface. In this paper we show that the present theory is in good agreement with JET ICRH experiments.

The modelling of ICRH can be broken down into three main parts: coupling of the wave into the plasma; propagation and absorption of the wave in the plasma; and the evolution of the velocity distribution of the resonating species. Wave propagation and power absorption are often calculated with ray tracing codes [3,4] or global wave codes [5-7]. The velocity distribution is either calculated with Fokker-Planck codes [8-10] or by using orbit following Monte Carlo codes [11]. The coupled wave spectrum depends not only on the geometry of the antenna but also on propagation and absorption of the waves. The absorption depends on the velocity distribution which in its turn depends on the absorbed power. Thus, the three problems should be solved self-consistently. In principle this can be done by coupling a global wave code with a Fokker-Planck code or a Monte Carlo code and solving the problem by iterations. However, such a combined code require large amounts of CPU time and is therefore not suitable for routine analysis of discharges. In order to obtain a code which is sufficiently fast to enable routine analysis we have instead used simplified models of the power deposition and velocity distributions. For calculating the flux surface averaged power density we

use the model described in Refs. [12,13] based on analysis with the global wave code LION [6]. The velocity distribution which usually becomes strongly anisotropic due to the preferential acceleration of the perpendicular velocity component and due to the low collisionality, is calculated using a model of the pitch-angle averaged velocity distribution and a model for the parallel velocity distribution. These models have been bench-marked against the bounce-averaged Fokker-Planck code BAFIC [10]. By using such simplified models, the ICRH power deposition can be practically modelled and compared with experimental results. A time dependent code called PION-T, based on these models, has been developed [1].

A major difficulty which appears when validating theory by comparing it with experimental results is that direct measurements of power deposition and velocity distributions are not normally available. Various methods have been developed for measuring the power deposition e.g. by measuring the time derivatives of the electron temperature after sawtooth crashes [14] or by modulating the power [15]. Because of the similar time scales for indirect electron heating by high energy ions and for transport processes, these methods require that the transport is modelled too, making them more ambiguous. In case of discrepancies it may be difficult to determine whether it is the heating or the transport which deviates from the model. The transport processes are also less well known. Therefore, these methods of measuring the power deposition are more suitable for studying direct electron heating, which occurs on a much faster time scale, for which the heating response can be separated from the transport.

If the density and the temperature profiles of the electrons and the ions can be measured, quantities such fusion yield and anisotropic energy content of the heated ions can be used for validating ICRH codes avoiding the problem with uncertainties in the transport processes. The fusion yield can be obtained by measuring gamma radiation or neutrons from fusion reactions involving the resonating ion species [16]. The anisotropic energy content can be obtained by

combining signals from different diagnostics measuring the plasma energy content. This is possible since the weight put on the parallel and perpendicular energy content varies between the diagnostics. Owing to the relatively few measured quantities which can be compared, different power depositions and velocity distributions could give rise to similar values of these quantities. By comparing different heating scenarii with different power deposition profiles, possible discrepancies between existing models and experimental results can be discovered. Previously the calculated fusion yield due to (He^3,D) reactions and fast energy content have been used to validate the PION code for steady state conditions [18]. The version of the code used for these calculations provided time independent self-consistent solutions of the power deposition and velocity distribution during ICRH. Good agreement between theory and experiments was found when steady states were reached at moderate power levels. These results were consistent with classical slowing down of high energy ions on electrons.

Often the discharges are too transient to be modelled with a steady state code. Equilibriation of the absorbed power during ion cyclotron frequency heating occurs on multiple time scales, electron heating via high energy ions take place on the time scale of fast ions slowing down on electrons. For typical JET parameters this time scale is of the order 0.1-1.5s and is comparable with that of the energy and the particle confinement times on which the equilibrium parameters evolve. By making time dependent simulations of discharges where power or equilibrium quantities change on the time scale of the slowing down time or faster we can obtain further information to be used for validating the codes and the underlying ICRH theories. With the time dependent PION-T code it is possible to compare the time evolution of fusion yield and fast ion energy content with experimental measurements in particular in connection with transient phenomena such as sawtoothing. The rapid reduction of the fast ion energy content after a sawtooth crash is analysed with the code. By calculating the energy distribution of the resonating ions we have found that the change in fast ion energy can be explained

by slowing down of fast ions having been expelled from the centre of the plasma to the outside of the q = 1 surface. Because the expelled ions collide with colder electrons the slowing down becomes much faster which reduce the energy of the high energy ions. These results are consistent with earlier results that a fraction of the high energy ions are expelled from the centre after a sawtooth crash [18].

In this report we compare results from the PION-T code with experimental results for minority heating of hydrogen at the fundamental cyclotron frequency in a majority deuterium plasma. The physics of this scenario is complicated by the fact that the hydrogen resonance coincides with the second harmonic resonance of deuterium. Both the hydrogen ions and the deuterium ions will therefore absorb the wave power at the same location. The partition of the absorbed power between these two species is sensitive to the hydrogen concentration. For the second harmonic deuterium absorption to be strong, a high deuterium temperature is required since it is a finite gyro radius effect. For low hydrogen concentrations the deuterium ions will be directly heated by the wave and a high energy tail formed which can enhance the neutron yield originating from (D,D) reactions. The second harmonic tail formation can then be assessed by monitoring the 2.4 MeV neutron flux and comparing it with the thermal yield. Because of the difficulties of getting rid of hydrogen and the requirement of a high deuterium temperature second harmonic heating of deuterium is rather sparsely observed.

Since the cyclotron heating acts preferentially in the perpendicular direction in velocity space a large fraction of the heated ions becomes trapped in wide banana orbits for high power densities. The assumption that the heated ions stay approximately on a flux surface then no longer holds. When comparing the calculated fast energy content with measurements we obtain good agreement for low power levels using a Fokker-Planck code without finite orbit effects. For large power levels we obtain a clear deviation, in particular in the later phase of the heating pulse when the tail is fully developed. When the finite deviation between

the drift orbits and flux surfaces are included we obtain good agreement for higher power levels as well.

2 MODELLING OF POWER DEPOSITION AND VELOCITY DISTRIBUTION

The power deposition depends on the strength and polarization of the wave field as well as on the local absorption. The latter depends on the velocity distribution which in its turn depends on the power deposition. Hence the power deposition and velocity distributions should be solved self-consistently. For steady state calculations in the absence of orbit effects this was done by iterating the power deposition calculated with a simple model and using a Fokker-Planck code solving the steady state velocity distribution [18]. Here we use a similar procedure but with a Fokker-Planck code solving the time dependent velocity distribution which can also include the deviation of a drift orbit from a flux surface [1,2].

When calculating the power deposition the antenna current is Fourier decomposed in the toroidal direction. The power deposition is then calculated for each toroidal mode with a model, where the power deposition is determined by the single pass absorption coefficients along the cyclotron layer and the averaged parallel velocity of the ions [12,13]. The model can then be used to calculate the power deposition for a non-Maxwellian velocity distribution. It also takes into account electron absorption by electron Landau damping and transit time magnetic pumping. The power deposition model has been compared with the LION code and good agreement is found [12,13]. Regarding the details of the power deposition calculations we refer to previous works [1, 2, 18].

Assuming the drift orbit of the resonating ions to coincide with a flux surface the velocity distribution during ICRH can be obtained by solving a Fokker-Planck equation including a quasi linear RF-operator.

$$\frac{\partial f}{\partial t} = C(f) + Q(f) \qquad (1)$$

where C is the collision operator and Q the RF-operator. The velocity distribution becomes highly anisotropic for large velocities. This is because the collision frequency decreases with energy and that the cyclotron absorption preferentially heats the ions in the perpendicular direction during intense heating. In spite of the large anisotropy it turns out that the pitch-angle averaged velocity distribution is well described by the solution of the following equation [19],

$$\frac{\partial F}{\partial t} = \frac{1}{v^2}\frac{\partial}{\partial v}\left\{[-\alpha v^2 + \frac{1}{2}\frac{\partial}{\partial v}(\beta v^2)]F\right\} + \frac{1}{v^2}\frac{\partial}{\partial v}\left[v^2 H(\frac{k_\perp v}{\omega_{ci}})\frac{\partial F}{\partial v}\right] \qquad (2)$$

where

$$H = \frac{1}{2}\int_{-1}^{1} K \left| J_{n-1}\left(\frac{k_\perp v}{\omega_{ci}}\sqrt{1-\mu^2}\right) + \frac{E_-}{E_+} J_{n+1}\left(\frac{k_\perp v}{\omega_{ci}}\sqrt{1-\mu^2}\right)\right|^2 d\mu$$

$$\alpha = \langle \Delta v_{||} \rangle + \frac{1}{2v}\langle (\Delta v_\perp)^2 \rangle$$

$$\beta = \langle (\Delta v_{||})^2 \rangle$$

and K is proportional to $|E_+|^2$ [19]. By keeping the Bessel functions unexpanded we take the gyro orbit corrections to all orders into account, which is of importance when the gyro orbits becomes comparable to the wavelength. The Coulomb diffusion coefficients α and β derived by Spitzer can be found in Ref. [20,21] for ions colliding with Maxwellian ions and electrons. The changes in velocity $\Delta v_{||}$ and $\Delta v_\perp$ refer here to the change in the direction to that the particle had before the collision.

When comparing isotropic moments such as power transfer to the background plasma species and fusion yield, calculated with this model of the pitch angle

averaged velocity distribution and the two dimensional BAFIC code, good agreement has been found [19]. There are mainly two reasons to why the approximate equation for F(v) above gives good agreement with full 2D calculations. First, for low powers the distribution is almost isotropic and Eq. (2) gives approximately the correct solution to F(v). Secondly, at higher powers most of the ions are contained in a high energy tail. Since the dominant collision process for such high energy ions is the slowing down on electrons, the energy of the tail is approximately given by $p_{RF}\, t_s / 2$, where p_{RF} is the RF-power density and t_s is the slowing down time for ion electron collisions [21]. Thus, the energy of the tail is independent of the details of the RF-operator.

The averaged parallel velocity, with respect to the magnetic field, is calculated according to the following formula [22]

$$\langle v_{||}^2 \rangle = \int_0^\infty \mu_{eff}^2 \, F(v) 4\pi \, v^2 dv \qquad (3)$$

where

$$\mu_{eff}^2 = \frac{1}{3}\left[1+\left(\frac{v}{v^*}\right)^2\right] / \left[1+\left(\frac{v}{v^*}\right)^2+\left(\frac{v}{v^*}\right)^4\right]$$

with $v^* = 0.5\, v_\gamma$ where v_γ is the characteristic velocity above which pitch angle scattering becomes weak [21]. The relation between v^* and v_γ is obtained by comparing $\langle v_{||}^2 \rangle$ calculated according to Eq. (3) and by direct solving the 2D-velocity problem with the BAFIC code [22]. One might intuitively think that the velocity distribution will be strongly affected by the presence of trapped particles, which are not properly accounted for in Eq.(4). In particular as the resonating ions with the highest energy are trapped and have their turning point close to the cyclotron layer. Because of the much smaller parallel velocity at the cyclotron layer than the averaged along the orbit these ions are then expected to absorb more

energy than passing particles. However, it turns out that the influence of this effect on the absorption strength is rather small [23,24].

The velocity distribution affects the power deposition in two ways: the parallel velocity distribution determines the Doppler broadening and thereby the radial width of the resonance layer; the perpendicular velocity distribution is important for the higher order gyroradius corrections of the absorption. For second harmonic heating gyro orbit effects enters already in the leading order term. These effects are taken into account by modelling the absorption coefficients as follows. The absorption coefficient in a planar geometry is given by

$$a(\psi) = \frac{\omega}{2P_x}\int \mathrm{Im}(\mathbf{E}^*\boldsymbol{\varepsilon}\mathbf{E})dx, \tag{4}$$

where the values of temperature and density used in calculating the dielectric tensor $\boldsymbol{\varepsilon}$ are defined by the flux surface ψ, the magnetic field strength is assumed to be inversely proportional to the major radius. The geometry is oriented so that the x-direction is across the absorption layer, z is in the direction of the magnetic field and P_x is the incident Poynting flux. The * denotes the complex conjugate quantity. In the absence of mode conversion the absorption coefficient for the various plasma species can be straightforwardly calculated with the WKB method giving for a Maxwellian plasma

$$a_\alpha(s) = \int_{-\infty}^{+\infty} \frac{da_\alpha}{dx}dx = \int_{-\infty}^{+\infty} \frac{k_0^2}{|k_\perp|}\left\{ \mathrm{Im}(\varepsilon_{xx}^\alpha)\left|\frac{\varepsilon_{xy}}{\varepsilon_{xx}-N_{||}^2}\right|^2 \right.$$

$$\left. + \mathrm{Im}(\varepsilon_{xy}^\alpha) + 2\,\mathrm{Re}(\varepsilon_{xy}^\alpha)\,\mathrm{Im}\left[\frac{\varepsilon_{xy}}{\varepsilon_{xx}-N_{||}^2}\right]\right\} \exp\left[-\int_{-\infty}^{x} 2\,\mathrm{Im}(k_\perp(x'))\,dx'\right]dx \tag{5}$$

To calculate the single pass absorption coefficients for a non-Maxwellian plasma we note that the local power absorption can either be calculated from the dielectric tensor as

$$p_{f\alpha} = \frac{\omega}{2\pi} \mathrm{Im}\,(\mathbf{E}^* \boldsymbol{\varepsilon}_\alpha \mathbf{E}) \tag{6}$$

or by using the quasi-linear RF-operator Q as

$$p_{f\alpha} = \int \frac{mv^2}{2} Q(f_\alpha) d^3v. \tag{7}$$

For an arbitrary velocity distribution we calculate $\langle v_\parallel^2{}_\alpha \rangle$ from Eq.(3). The absorption strength in the power deposition calculation is made to agree with that of the Fokker-Planck calculation by using the following procedure: calculate the dielectric tensor, $\boldsymbol{\varepsilon}_{0\alpha}$, including absorption to the lowest non-vanishing order in $k_\perp v/\omega_{ci}$ and the locally absorbed power $p_{0\alpha}$ for a bi-Maxwellian velocity distribution with the same density and parallel temperature as the actual distribution but with the perpendicular temperature equal to the background ion temperature. We then calculate

$$\gamma_\alpha = \frac{p_{f\alpha}}{p_0} \tag{8}$$

and

$$\gamma_t = \frac{\sum \gamma_\alpha [da_{\alpha 0}/dx]}{\sum [da_{\alpha 0}/dx]} \tag{9}$$

where $p_{f\alpha}$ is the power absorbed by the actual velocity distribution obtained from Eq.(7) and $a_{\alpha 0}$ is the absorption coefficient obtained from Eq.(5) with $\boldsymbol{\varepsilon}_{0\alpha}$ as the dielectric tensor. The actual absorption coefficient is then obtained by multiplying the integrand of Eq.(5) with γ_α and replacing $\mathrm{Im}(k_\perp)$ with $\gamma_t\ \mathrm{Im}((k_\perp))$ but still using $\boldsymbol{\varepsilon}_{0\alpha}$ as the dielectric tensor. With this procedure we avoid calculating the actual dielectric tensor, which is more complicated.

The modification of the absorption due to changes in the velocity distribution is included in the time dependent PION-T code as follows: at the beginning of each time step the parameters $\langle v_\parallel^2{}_\alpha \rangle$, γ_α and γ_t are evaluated from the distribution function; a power deposition is produced; $k_\perp$ and the ratio $|E_- / E_+|$ is calculated; the evolution of the velocity distribution is then calculated during each time step keeping the power deposition fixed; from the velocity distribution at the end of the time step, i.e. at the beginning of a new time step, a new set of parameters $\langle v_\parallel^2{}_\alpha \rangle$, γ_α and γ_t is evaluated and a new power deposition is calculated; this procedure is repeated until the end of the calculation.

The effect of that a drift orbit deviates from a flux surface is taken into account in a modified version of the code called PION-TO. In this version, the collision coefficients, α and β in Eq.(3), are bounce averaged for each energy over a typical drift orbit i.e. an orbit, having its turning point close to the cyclotron resonance. In the calculation of flux surface averaged velocity space moments, such as the energy density and the collisional power transfer to the background species, the finite widths of the drift orbits are also taken into account. For further details see Ref.[2].

3 SIMULATIONS OF ICRH HEATING ON JET AND COMPARISON WITH EXPERIMENTAL RESULTS.

In this section we compare code simulations with experimental results for hydrogen minority heating in deuterium majority plasmas. The two quantities which we compare with experimental measurements are the neutron yield and the

fast ion energy content. The enhancement of the neutron yield above the thermal level can be used to access the tail formation of the deuterium during second harmonic heating. The fast ion energy content, W_f, is here defined as the perpendicular energy content in excess of two times the parallel value. This quantity provides information about the fast ions since, as a result of the preferential heating of the perpendicular velocity component, an anisotropic high energy tail is formed during ICRH. It is possible to measure W_f by taking the difference between two different measurements of the plasma energy putting different weight to the parallel and perpendicular energy e.g.

$$W = \frac{3}{4}(W_{DIA}-W_{MHD}) = W_{\perp}-2W_{||} = W - 3W_{||} \tag{10}$$

where

$$W_{DIA} = \frac{3}{2}\ W_{\perp} \tag{11}$$

and

$$W_{MHD} = \frac{3}{4}\ W_{\perp} + \frac{3}{2}\ W_{||} \tag{12}$$

W_{DIA} is measured by the diamagnetic loop and W_{MHD} is obtained form other magnetic measurements together with MHD equilibrium calculations. In some cases there can be a certain offset between these two measurements, which has to be compensated for. In the absence of ICRH these two measurements of the plasma energy agrees fairly well [17]. The parallel energy content is dominated by the isotropic bulk ion distribution and the electron distribution. An enhancement of the parallel energy of the minority ions above the thermal level appears because of pitch angle scattering as accounted for by Eq. (3) and because of the variation of the magnetic field along the particle orbit. However, the perpendicular energy is the dominating one.

For calculating the RF-power deposition profile and neutron yield the following data were used: The electron temperature, measured from the electron cyclotron emission [25]; the ion temperature, from the X-ray crystal spectrometer measuring radiation from NiXXVII [26] (Note that the time resolution of the data from the X-ray cyrstal is not high enough to properly resolve the sawteeth); electron density from an infrared interferometer [27]; and Z_{eff} from visible Bremsstrahlung [28]. When comparing code calculations with experimental data, the code is set up so that it takes all its input data directly from the JET pulse file system. The only data required for the calculations which is not available with reliable accuracy is the hydrogen concentration. However, we have found that for the hydrogen minority in deuterium scenario the calculated W_f is not too sensitive to the minority concentration which is one of the reasons to why we have chosen to analyze this scenario. On the other hand, the neutron yield is very sensitive to the minority concentration.

3.1 Comparison between PION-T and experimental results

We start by analyzing discharge #19650, for which we obtain some clear second harmonic heating, but for which the power per particle is so low that the orbit effects are small. The influence of orbit effects will be studied in section 3.2. The evolution of central electron temperature, ion temperature, electron density, ion density and coupled RF-power are shown in Fig. 1 during the RF-heating phase for #19650. The vacuum magnetic field at the centre of the plasma chamber was $B_0 = 3.1T$ and the RF-frequency 48MHz. The slowing down time, which characterize the formation time of the high energy tail, was for hydrogen in the centre at the beginning of the heating phase $t_s = 0.15s$ and at $t = 8s$ it was 0.4s. In the simulations we have choosen $n_H/n_D = 0.06$ which has been fitted to give good agreement with the neutron flux.

The time evolution of the calculated powers, absorbed by hydrogen, deuterium, electron absorption, and total coupled power are shown in Fig. 2a. The electron

absorption which only accounts for 10% of the absorbed power takes place by electron Landau damping and transit time magnetic pumping. Whereas the hydrogen absorption decreases slowly after t = 7.5 s, the second harmonic absorption increases throughout the entire heating pulse. This is a consequence of the development of a deuterium tail which increases the second harmonic absorption. Because of the high hydrogen concentration the second harmonic absorption accounts only for about 6% of the total absorbed power. Even though the power absorbed by hydrogen decreases, the total collisional electron heating from high energy ions remains fairly constant as can be seen in Fig. 2b, where the time variation of the power transfers to the electrons and ions are shown. The reduction of power transfered to the electrons from the hydrogen ions is partly compensated for by the power transfered from the deuterium tail. The flux surface averaged power absorption profiles are shown in Fig. 3a at t = 9.4s. The deuterium absorption profile is more peaked than the other absorption profiles. The profile of the power transfered to electrons and ions are shown in Fig.3b. The power transfered to the ions has a profile with a double peak. The highest power density peak near the centre comes from deuterium heating and the lower flat peak further out arises from heating by hydrogen. The comparison between measured and calculated fast energy content is shown in Fig. 4. We note that not only the steady state value, but also the time evolution of the fast energy content is well described giving further support for classical slowing down of high energy ions. To assess how sensitive the results are to the width of the calculated power deposition profile we compare the results with that for power deposition profiles of the form

$$P(s) = P(1)\ \frac{1-\exp\left[-\left(\frac{s-s_1}{s_0}\right)^2 \ln 2\right]}{1-\exp\left[-\left(\frac{1-s_1}{s_0}\right)^2 \ln 2\right]} \qquad s > s_1$$

$$P(s) = 0 \qquad s < s_1 \qquad (13)$$

where s_1 has been chosen so that the modelled power deposition peaks at the same position as the power deposition calculated by the PION-T code. P(1) is the coupled power and s_0 the width. The comparison for different values of the parameter s_0 = 0.1, 0.2, 0.3 and 0.4 are also included in Fig.4. The self-consistent calculations is close to s_0 = 0.2. A more narrow as well as a broader power deposition profile give a clear discrepancy between the measured and the calculated fast energy content. Thus, the fast energy content can be used to assess the accuracy of the calculated power deposition.

Next we compare the calculated and measured neutron flux from D-D reactions. In the absence of ICRH the measured yield agrees well with the calculated thermal yield. In the presence of ICRH the yield is about 20% higher than the calculated thermal yield, i.e. the yield obtained when the deuterium distribution is assumed to be Maxwellian, see Fig.(5). The thermal yield has a decreasing trend caused by a decreasing deuterium density and a fairly constant temperature after t = 8.0s. The increasing discrepancy between the measured and calculated thermal yield seems only explainable by the formation of a high energy tail caused by second harmonic deuterium heating. It is interesting to note the very slow time scale on which the non thermal yield increases. In the code simulation this is a consequence of taking into account.enhanced absorption due to tail formation.

The partition between the power going to second harmonic cyclotron heating of deuterium and fundamental cyclotron heating of hydrogen is sensitive to the hydrogen concentration. The experimentally measured n_H/n_D ratio is rather uncertain. In Fig. 6 we compare the total calculated neutron yield with the measured one for hydrogen concentrations of 4% and 10%. The ratio n_H/n_D = 6% fits the experimentally measured neutron yield best. Lower hydrogen concentration gives a too large neutron yield whereas a higher concentration gives too low one. The calculated neutron reaction rate profiles are shown in Fig. 7 at t = 8.2s and

t = 9.4s. At the earlier time the second harmonic tail formation is small which is consistent with close agreement between the measured fusion yield and calculated thermal one. At t = 9.4 s the fusion reaction rate peaks strongly off-axis where the power density is highest.

3.2 Finite orbit correction for high power densities

For high minority concentrations or low power density the code simulations with the PION-T code and experiments agree well for the fast ion energy content, as can be seen in Fig. 8a for discharge #12295. For high power densities or for low minority concentrations, the deviation between the measured and calculated fast energy becomes large [29, 30], as can be seen in Fig. 8b for discharge #12298. For this situation the deviation between a drift orbit and a magnetic flux surface becomes large. When taking this effect into account, as in the PION-TO code described previously in section 2, good agreement is obtained which is shown in Fig. 8. The two discharges are characterized by the following parameters: plasma current 2MA, vacuum toroidal magnetic field B_0=2.2 T, RF-frequency 32.2MHz. The density and temperature were slightly different for these discharges, #12295 had a density and an electron temperature at the magnetic axis of $3.2 \cdot 10^{19}$ m^{-3} and 6.0 keV, respectively, at t = 8.0s and coupled a RF-power of 4.6MW; discharge #12298 had a density and an electron temperature at the magnetic axis of $3.6 \cdot 10^{19} m^{-3}$ and 7.0 keV, respectively, at t = 8.5s and coupled RF-power of 8.0MW; The corresponding slowing-down times were 0.60s and 0.63s, respectively.

In Fig. 9 we show the different power transfer profiles for #12298. The profile of power transferred to the electrons becomes a much broader when the orbit effects are included. On the other hand, since it is mainly low energy ions with small orbit widths that contribute, the power transfer profile to the background ions is almost unchanged. The fusion yields measured by the neutrons are for these discharges

not sensitive to the finite orbit width because the thermal contribution dominates completely.

3.3 Loss of fast ions during sawtooth crashes

The agreement between measurements and calculations of the fast energy content and fusion yield is for off-axis and low RF-power rather good. In particular during ramp-up of the RF-power and for sawtooth free periods. However, after a sawtooth crash a rapid reduction of the fast ion energy content is sometimes seen, which is larger than the calculated one. This can be seen in Fig. 4 for discharges #19650. The observed reduction of the energy content is larger than the one predicted by the PION-T code. The calculations take into account the reduction of the fast energy content after a sawtooth crash caused by the decrease of the slowing down time due to lower electron temperature, but this cannot explain the reduction. The deviation may be caused by expulsion of fast ions from the centre to the outer region where they will slow down faster because of a lower electron temperature. In order to test this, we assume that a fraction α of the fast ions inside the inversion radius are expelled after the crash and redistributed just outside the inversion radius. This is implemented in the simulations in the following way: Inside the inversion radius the non-thermal velocity distribution is reduced by a factor α and a thermal distribution is added to compensate for the expelled ions; between the inversion radius and the mixing radius a non-thermal distribution is added so as to conserve the total energy content. By varying α and comparing with experiments we can estimate how large this fraction is. Fig. 10 shows the comparison of fast energy traces after the crash for discharge # 19650 after t = 8.9s with α = 0.4 as calculated by the PION-TO code where orbit effects are included. The time variation of the fast energy agrees fairly well. Thus, the modelling is consistent with that about 60% of the fast energy content in high

energy ions remain inside the inversion radius after a sawtooth crash. The particles lost due to that their drift orbits intersect the wall or limiter either before or after a sawtooth crash are calculated to be too few to explain the reduction in fast energy. The flux surface averaged energy density of the resonating ions is shown in Fig.11 at various time step during the sawtoothing.

5 DISCUSSIONS AND CONCLUSION

The time dependent PION-T code, which calculates the ICRF-power deposition and velocity distribution of the resonating ions self-consistently, has been used for comparing simulations with measurements. The time evolution of the anisotropic plasma energy, caused by anisotropic high energy tails of the resonating ion species, and the neutron yield from D-D reactions enhanced by a deuterium tail caused by second harmonic heating have been compared. The code is based on the assumption of classical collisional heat transfer to the background plasma species and quasi-linear RF-absorption by resonating ions. Since the code is time dependent it is possible to analyse transient phenomena. Both during power ramp up and ramp down the fusion yield and fast energy content are well described by the code supporting classical slowing down. A possible faster slowing down or loss of high energy ions cannot be made compatible with that a larger fraction of the power is absorbed by cyclotron absorption since only a small fraction of the total power is absorbed by other mechanisms such as electron Landau damping and electron transit time magnetic pumping. Having found that classical slowing down is valid one can vary the power deposition to show that the calculated power deposition cannot be significantly different from the experimental one.

The second harmonic heating of deuterium is identified by comparing the time evolution of the fusion yield with the calculated thermal one. The thermal fusion yield is exceeded with about 20% for discharge #19650. It is difficult to find discharges with a neutron flux strongly exceeding the thermal flux during ICRH because a small amount of residual hydrogen are often present which reduce the

power absorbed by the deuterium. The enhanced fusion yield from second harmonic heating develops on a long time scale. This long time scale is due to the change in the power partition as the second harmonic tail develops. The deuterium absorption increases and the hydrogen absorption is reduced. The higher order finite Larmor radius terms are found to be important when explaining the time evolution.

For large amounts of coupled power, so that the calculated power density becomes high, the agreement between calculated and measured fast energy content becomes less good which has been reported earlier in [29, 30]. The analysis presented here shows that this deviation can for many discharges be explained by finite orbit effects. In particular, the resonating particles heated in the centre of the plasma achieve so wide banana orbits that they pass through regions with shorter slowing down times. For particles intersecting the cyclotron resonance further out, this effect becomes less important because of lower power density and lower electron temperature. The finite orbit width will reduce the fast energy content due to shorter effective slowing down times. It gives also rise to a broader power transfer profile. However, there are discharges for which it is difficult to obtain agreement even when orbits effects are included. In particular, for discharges with long slowing down time and high power. Other finite orbit effects such as the outward drift of the banana orbit and RF-induced diffusion will also reduce the fast energy content [11,31-33]. These effects are not included in the present analysis.

Noticeable deviations between measured and calculated values of fast energy content occur after sawtooth crashes in particular after long sawtooth free periods. This reduction can be explained by redistribution of a fraction of the high energy ions to the outside of the inversion radius, after a sawtooth crash. By varying the fraction lost and redistributing it outside the inversion radius we found the simulation to agree with the measurements if 40% of the fast ions are redistributed. A possibility would have been that the fast ions are redistributed and then lost by prompt losses due to their wide banana orbits. However, this has to be refuted

because of the number of ions having such wide banana orbit are too few to account for the reduction in the fast energy. The redistribution of about 40% of the high energy ions after a sawtooth crash is consistent with earlier analysis [18] where we compared the local electron heating after a sawtooth crash with calculations.

For ICRH one may expect velocity space instabilities to occur and reduce the anisotropy. However, this cannot have had any large effect, because the measured value of the fast energy content is consistent with the code simulations. In case the tail would have been more isotropic the total energy in the tail would have had to become larger which would have contradicted the simulations. However, a more isotropic tail could have been an alternative explanation of the reduction in the anisotropic tail seen during high power heating. Since the reduction due to orbit effects was clearly in quantitative agreement with the experiments, we conclude that a strong anisotropic velocity distribution is maintained during ICRH and instabilities caused by anisotropy are not sufficiently rapid to significantly isotropize the velocity distribution.

The orbit effects included in this report are found to be important for high power densities and long slowing down times giving rise to a much flatter electron heating profile than when the orbit effects are neglected. This effect can be important when evaluating the local transport coefficients from the measured temperature and density profiles, which will reduce the thermal electron diffusivity in the centre. Since the power transfered to the background ions comes from resonating low energy ions having small banana widths the corresponding profiles become less affected.

The most energetic resonating ions have similar or higher energies than the thermonuclear α-particles, one would therefore be tempted to draw the conclusion that they will behave similarly. However, there is one main difference between the distributions, during ICRH the distributions become very anisotropic with the

perpendicular energy being much greater than the parallel one, whereas the velocity distribution of the thermonuclear α-particles is expected to be isotropic. In the case of thermonuclear α-particles the parallel velocity will exceed the Alfvén wave velocity, global Alfvén waves are then expected to occur which may throw out these α-particles [34,35]. Because of the lower parallel velocity during ICRH the same instability should not occur. However, recently it has been predicted that also a high perpendicular tail should lead to excitation of global Alfvén waves and possible expulsion of high energy ions [36].

Acknowlegements

We are very grateful to D. Muir for providing the program which interface the PION-T code with the experimental data banks. Thanks are also due to H. Morsi for help with the ion temperature data. Finally, we would like to acknowledge valuable discussion with F. Porcelli concerning orbit effects.

References

[1] Eriksson, L.-G., Willén, U. and Hellsten, T., in "Theory of Fusion Plasmas" Eds. Vaclavik, J., Troyon , F. and Sindoni, E., Bologna 1990, p. 421.

[2] Eriksson, L.-G. and Porcelli, F., JET-R(91)11, JET Joint Undertaking, 1991.

[3] Brambilla, M., Computer Phys. Reports 4 (1986) 1.

[4] Koch, R., Bhatnagar, V.B., Messian, A.M. and van Ester, D., Computer Physics Communications 40 (1986) 1.

[5] Itoh, K., Itoh, S.-I. and Fukuyama, A., Nucl. Fusion 24 (1984) 13.

[6] Villard, L., Appert, K., Gruber,R. and Vaclavik, J., Computer Physics Reports 4 (1986) 95.

[7] Brambilla, M. and Krücken, T., Nucl. Fusion 28 (1988) 1813.

[8] Kesner, J., Nucl. Fusion 18 (1978) 78.

[9] Kerbel, G.D. and McCoy, M.G., Phys. Fluids 28 (1985) 3629.

[10] Succi, S., Appert, K., Core,W.G.F., Hamnén, H., Hellsten, T. and Vaclavik, J., J. Computer Physics Comm. 40 (1986) 137.

[11] Kovanen, M.A., Core, W.G.F. and Hellsten, T., Nucl. Fusion 32 (1992) 787.

[12] Hellsten, T. and Villard, L., Nucl. Fusion 28 (1988) 285.

[13] Hellsten, T. and Eriksson, L.-G., Nucl. Fusion 29 (1989) 2165.

[14] Eriksson, L.-G. and Hellsten, T., Nucl. Fusion 28 (1989) 875.

[15] Gambier, D.J., Evrard, M.P., Adams, J., Becolet, A., Corti, S., et al., Nucl. Fusion 30 (1990) 23.

[16] Sadler, G., Conroy, S. W., Jarvis, O. N., van Belle, P., Adams, J. Hawkes, M., Hone, M. A., Fusion Technology 18 (1990) 556.

[17] Christiansen, J. P., J. Comput. Phys. 73 (1987) 85.

[18] Eriksson, L-G,. Hellsten, T., Boyd, D.A., Campbell, D.J., Cordey, J.G., et al., Nucl. Fusion 29 (1989) 87.

[19] Anderson, D., Core, W.G.F., Eriksson, L-G., Hamnén, H., Hellsten, T. and Lisak, M., Nucl. Fusion 27 (1987) 911.

[20] Spitzer, L. Jr., The Physics of Fully Ionized Gases, 2nd Revised Edition, Interscience, New York (1962).

[21] Stix, T., Nucl. Fusion 15 (1975) 737.

[22] Anderson, D., Eriksson, L-G., Lisak, M., Plasma Phys. Controlled Fusion 29 (1987) 891.

[23] Hellsten, T., Appert, K., Core, W., Hamnén, H., Succi, S., et al., Proc. 12th European Conf. on Controlled Fusion and Plasma Physics (Budapest 1985) Vol. 9F, Part II, p. 124.

[24] Harvey, R. W., Kerbel, M.G., McCoy G. D., and Chiu, S. C.,

Nucl.Fusion 26 (1986)43.

[25] Costley, A. E., Baker, E. A. M., Brusati, M., et al., Proc. 12th European Conf. on Controlled Fusion and Plasma Physics (Budapest 1985) Vol. 9F, Part II, p. 227.

[26] Zastrow, K.-D., Morsi, H. W., et al., J. Appl. Phys. 10 (1991) 6732.

[27] Fessey, J. A., Gowers, G. W., Hugenholtz, C. A. J., Slavin, K., J., Phys. E Sci. Instrument., 20 (1987) 169.

[28] Morgan, P. D., et al., Rev. Sci. Instrum. 56 (5) part 2 (1985) 862.

[29] Cordey, G., Chistiansen, J. P., Core, W. G. F., Cottrell, G. A., Eriksson, L.-G., et al. Proc. 19th European Conf. on Controlled Fusion and Plasma Physics (Berlin 1991) Vol. 15C, Part III, p. 385.

[30] Thomas, P. and the JET team Proc. 12th Int. Conf. on Plasma Physics and Controlled Nuclear Fusion Research, Nice, France 1988.

[31] Hellsten, T., Plasma Physics and Controlled Fusion 31 (1989) 1391.

[32] Chen, L., Vaclavik, J. and Hammett, G., Nucl. Fusion 28(1988) 389.

[33] Riyopolulos, S., Tajima., T., Hatori, T. and Pfirsch, D., Nucl. Fusion 26 (1986) 43.

[34] Li, Y. M., Mahajan, S. M. and Ross, D. W., Phys. Fluids 30 (1987) 1466.

[35] Fu, G. Y., van Dam, J. W., Phys Fluids B 1(1989)1949.

[36] Wilson, J., R. Budney, R., Bell, M. G., Fredrickson, E., Hosea, J., et al., Proc. 12th Int. Conf. on Plasma Physics and Controlled Nuclear Research, Fusion, Würzburg, Germany,1992 E-2-2.

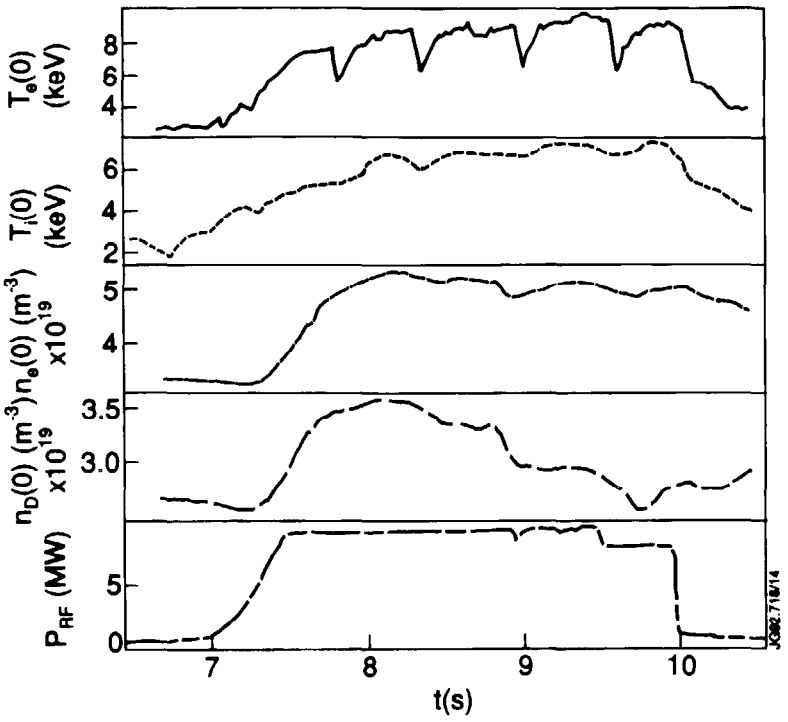

Fig. 1 Time evolution of the plasma parameters in discharge #19650. Central electron temperature, T_e; central ion temperature, T_i; electron density at magnetic axis, n_e; deuterium density at the magnetic axis n_D, coupled ICRH power, P_{RF}.

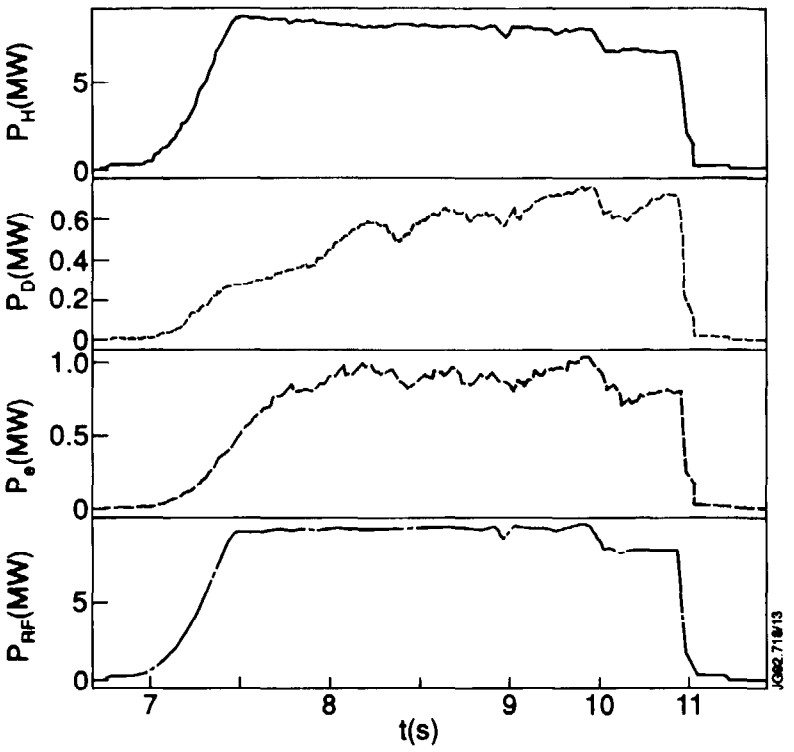

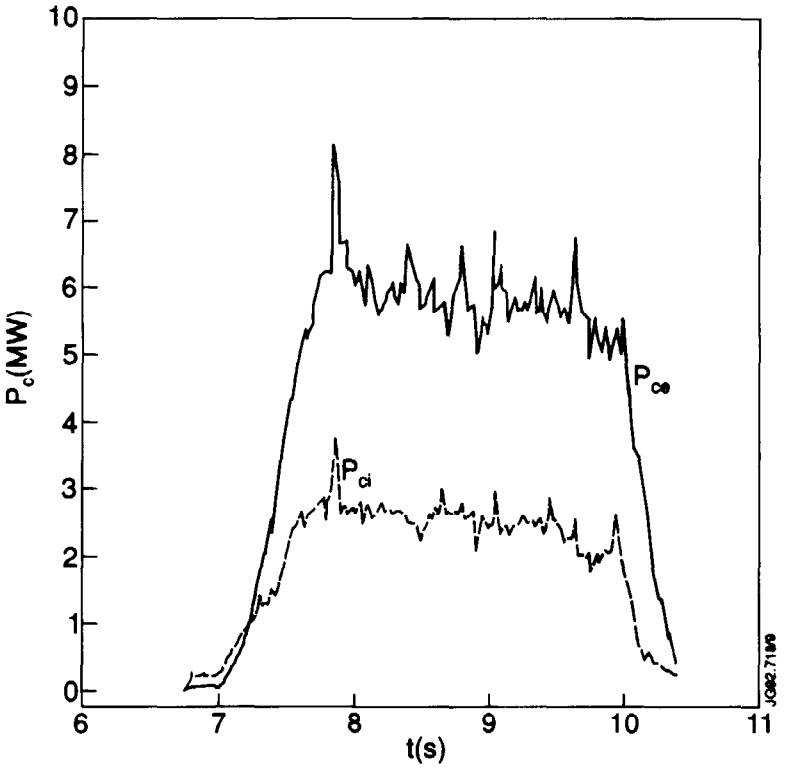

Fig. 2 a) Time evolution of the power absorbed by hydrogen P_H, deuterium P_D, electrons P_e and total coupled power P_{RF}.

b) collisional power transfer to ions, P_{ci} and electrons, P_{ce}.

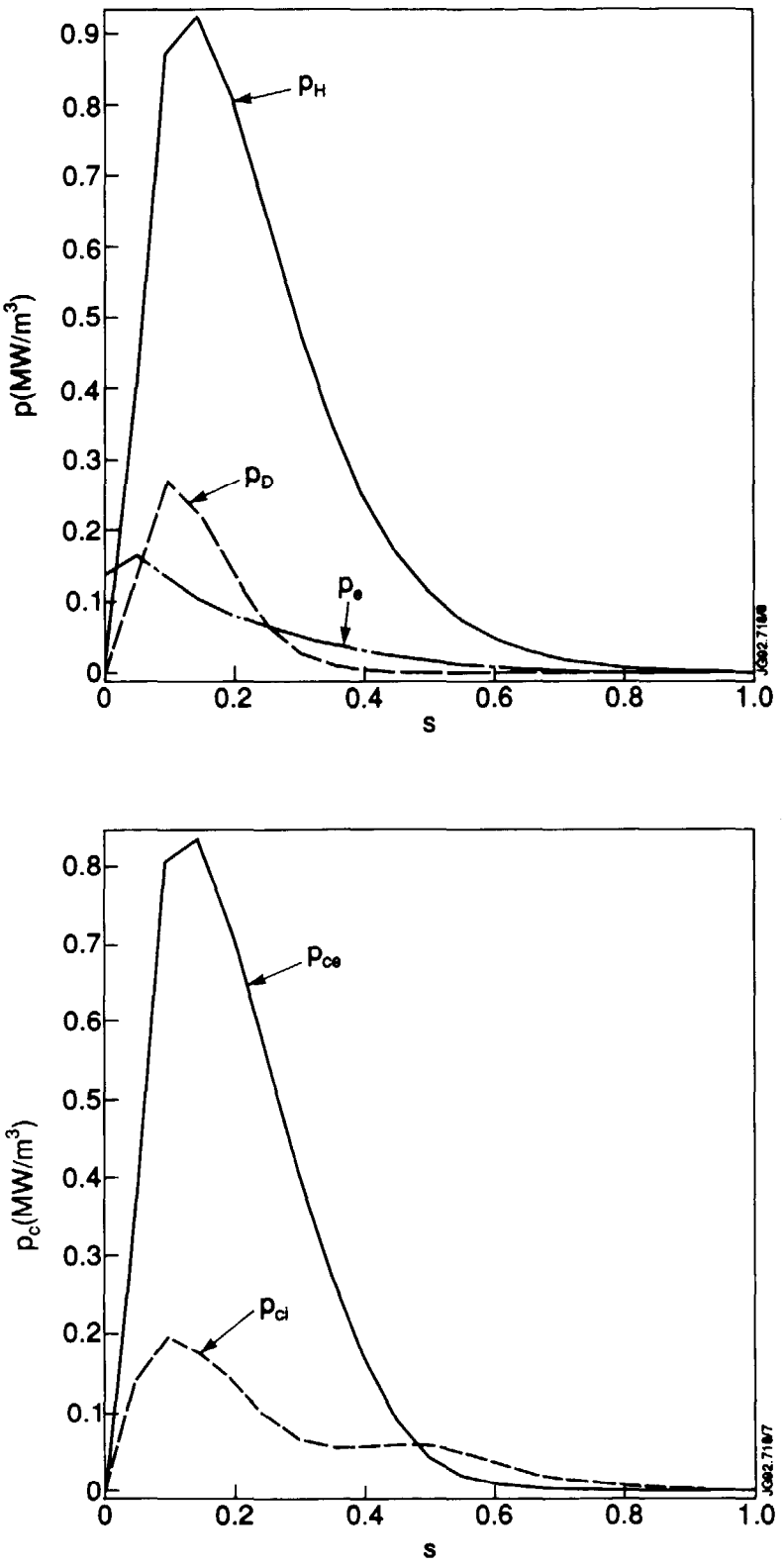

Fig. 3 a) Calculated flux surface averaged absorption profile of hydrogen absorption, p_H, deuterium absorption, p_D, and electron absorption, p_e at t = 9.4s for #19650.

b) Calculated flux surface averaged collisional power transfer profiles to ions, p_{ci}, and electrons, p_{ce}.

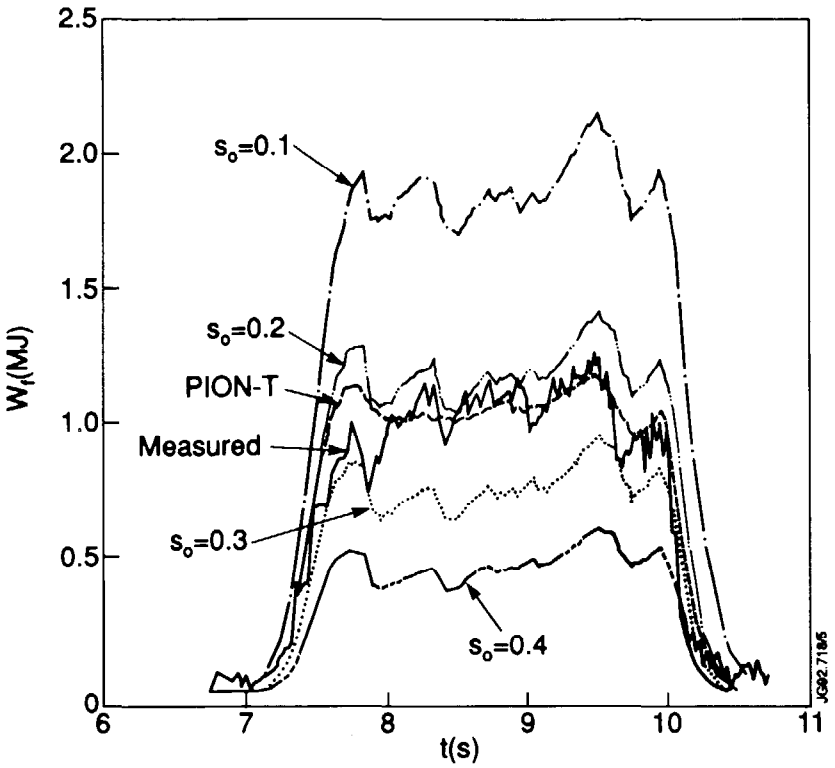

Fig. 4 Fast ion energy content of discharge # 19650 defined by Eq. (10) versus time, measured and calculated with the PION-T code . The curves indicated by s_0=0.1, s_0=0.2, s_0=0.3 and s_0=0.4 are for the power depositions profiles described by Eq. (13) with the corresponding s_0 value.

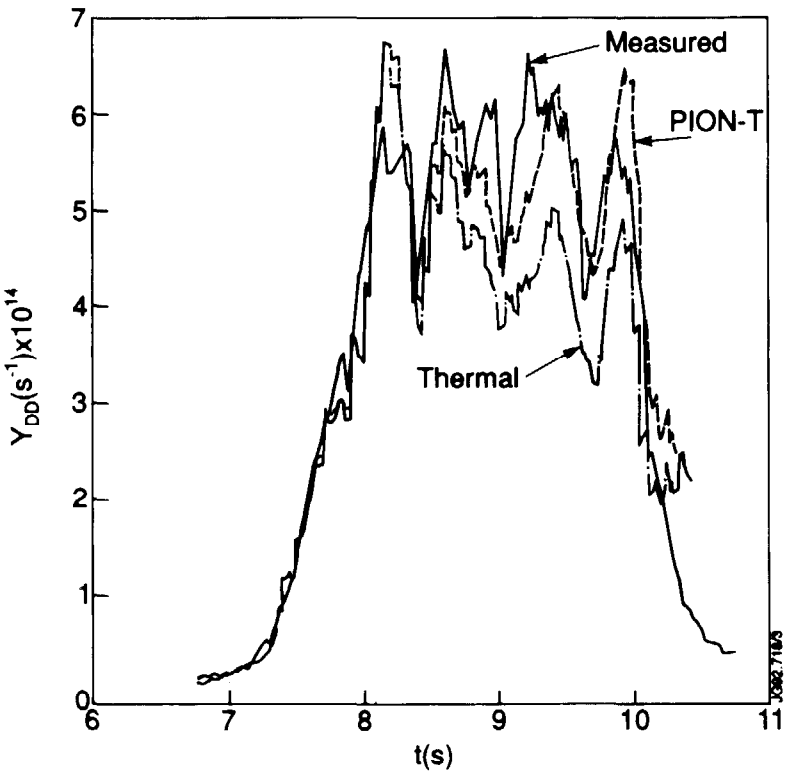

Fig. 5 Comparison between measured and calculated neutron flux including second harmonic heating and thermal neutron flux.

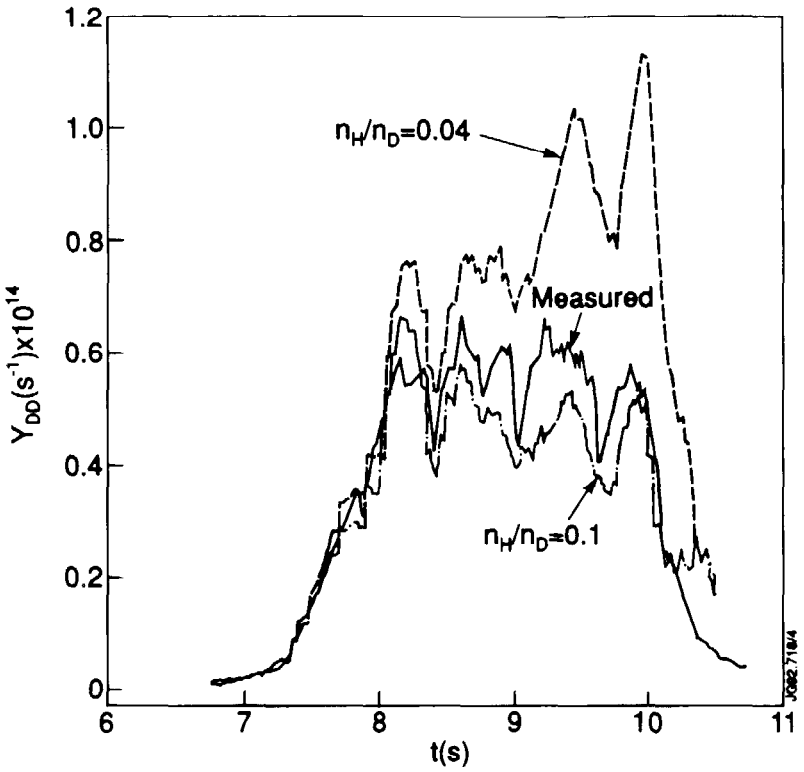

Fig. 6 Comparison between measured and calculated neutron flux for different hydrogen concentrations.

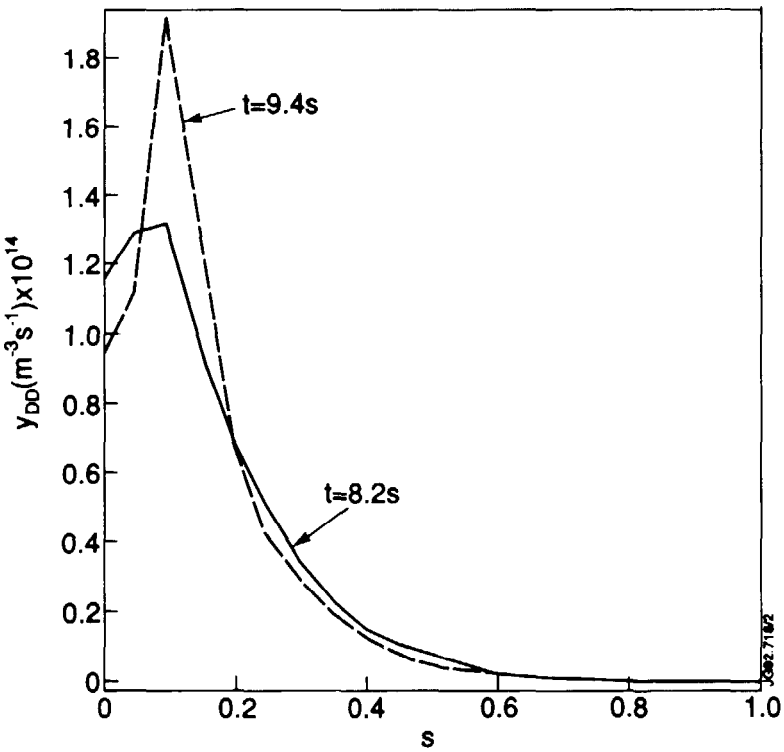

Fig. 7 Calculated flux surface averaged reaction rate at t=8.2 s and t=9.4 s.

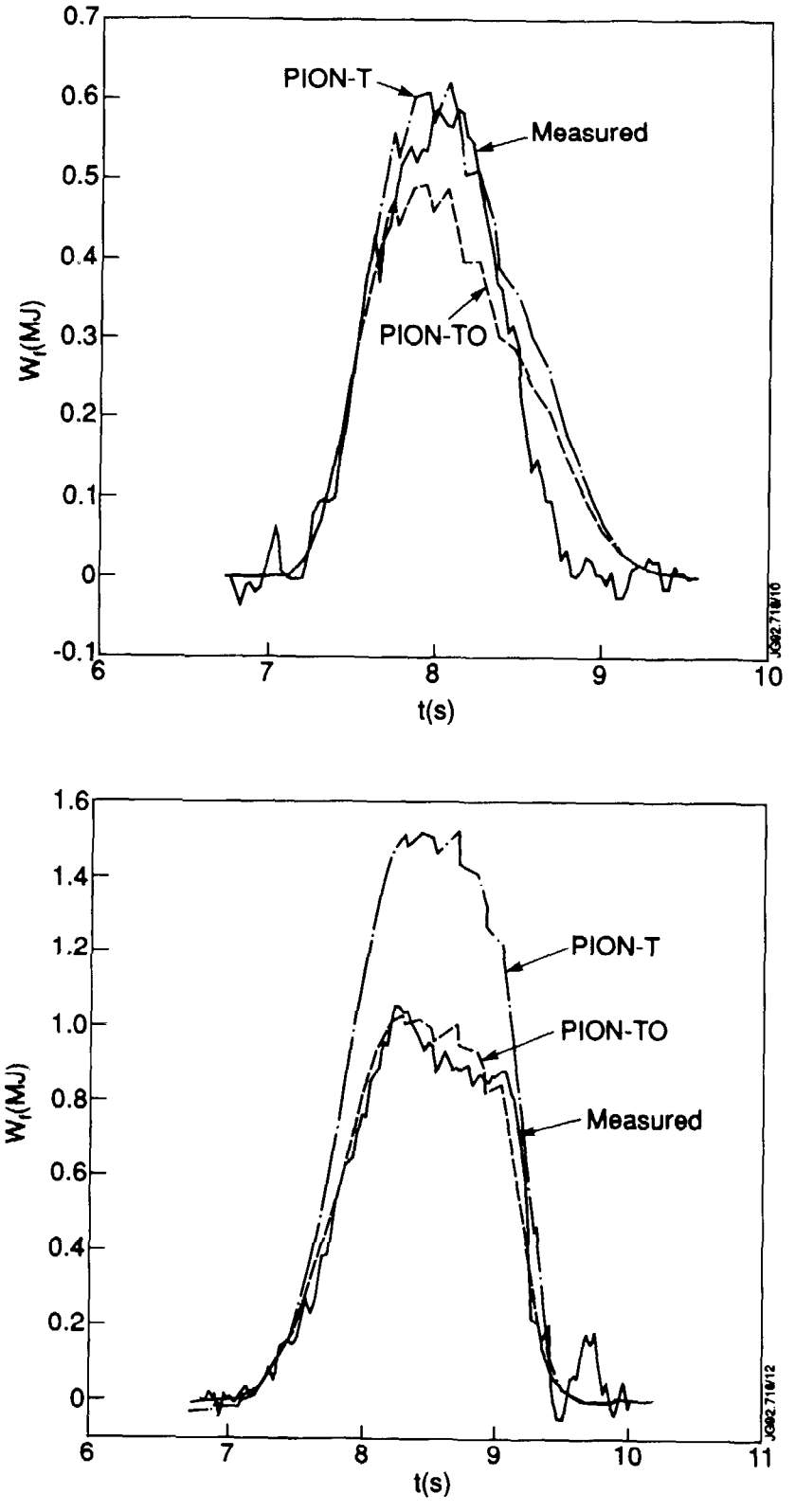

Fig. 8 Comparison of fast ion energy content measured and calculated with the PION-T and PION-TO codes. The latter code includes finite orbit effects. a) discharge #12295 b) discharge #12298.

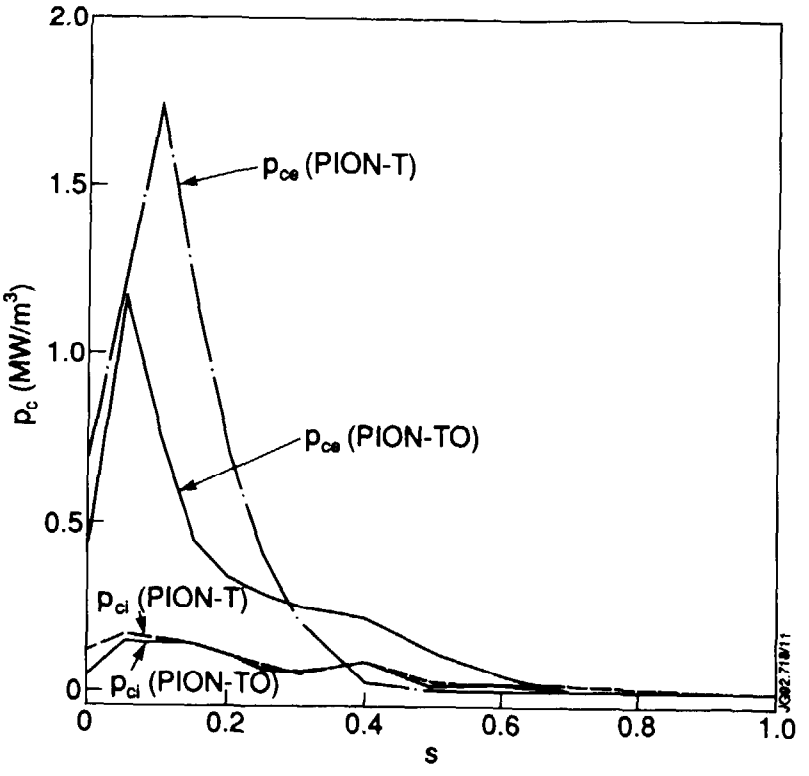

Fig. 9 Calculated flux surface averaged power transfer profiles for #12298 without finite orbit effects (PION-T) and with finite orbit effects (PION-TO).

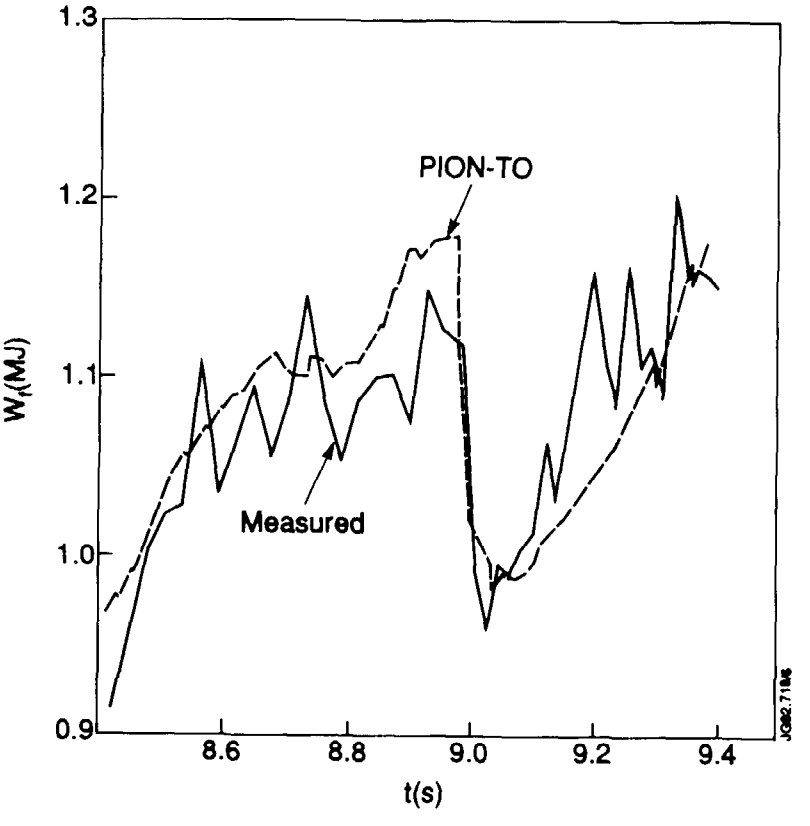

Fig. 10 Comparison of fast ion energy content for discharge #19650 after a sawtooth crash, measured and calculated with PION-TO assuming that 40% (a = 0.4) of the fast ion inside the inversion radius are expelled.

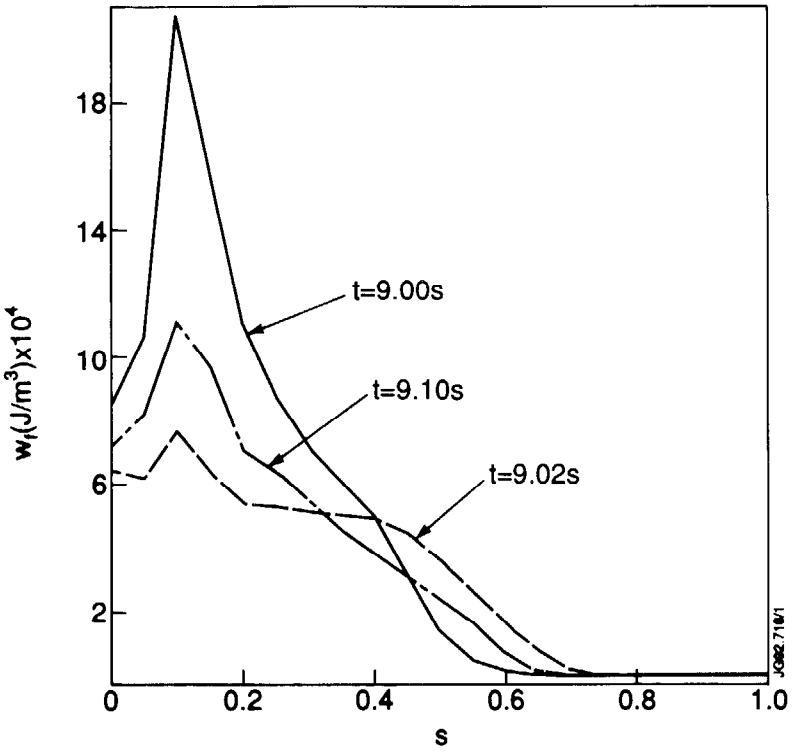

Fig. 11 Simulation of the flux surface averaged energy density, w_f, of fast ions for discharge #19650 before and after the sawtooth crash at t = 9.0s.